Electronic Supplementary Information

Crystallization, structural diversity and anisotropy effects in 2D arrays of icosahedral viruses

M. Fukuto, Q. L. Nguyen, O. Vasilyev, N. Mank, C. L. Washington-Hughes, I. Kuzmenko, A. Checco, Y. Mao, Q. Wang, and L. Yang

I. MEASURED ISOELECTRIC POINT OF TYMV

See Fig. S1.

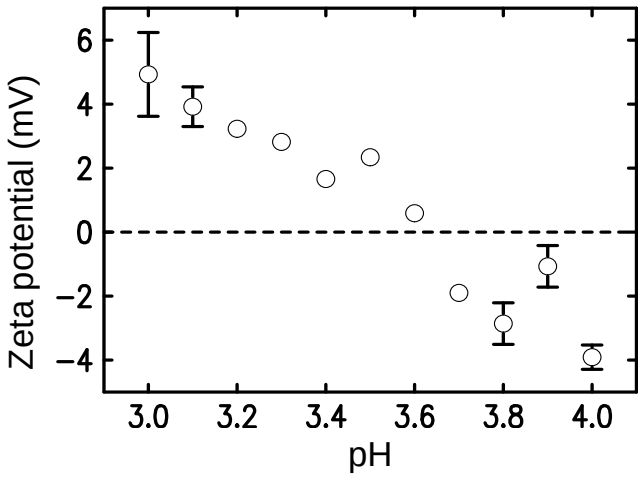

FIG. S1: The isoelectric point of TYMV was determined through zeta potential measurements on TYMV in 10 mM citric acid solutions as a function of pH (±0.1), using a Zetasizer light scattering set-up (Malvern corporation) as previously described [1]. The concentration of TYMV used was 0.015 mg/ml, the same as for most of the x-ray measurements. The data show that the isoelectric point is pI $= 3.6 \pm 0.1$, consistent with the previously reported values [2].

II. ADDITIONAL GISAXS DATA

See Fig. S2.

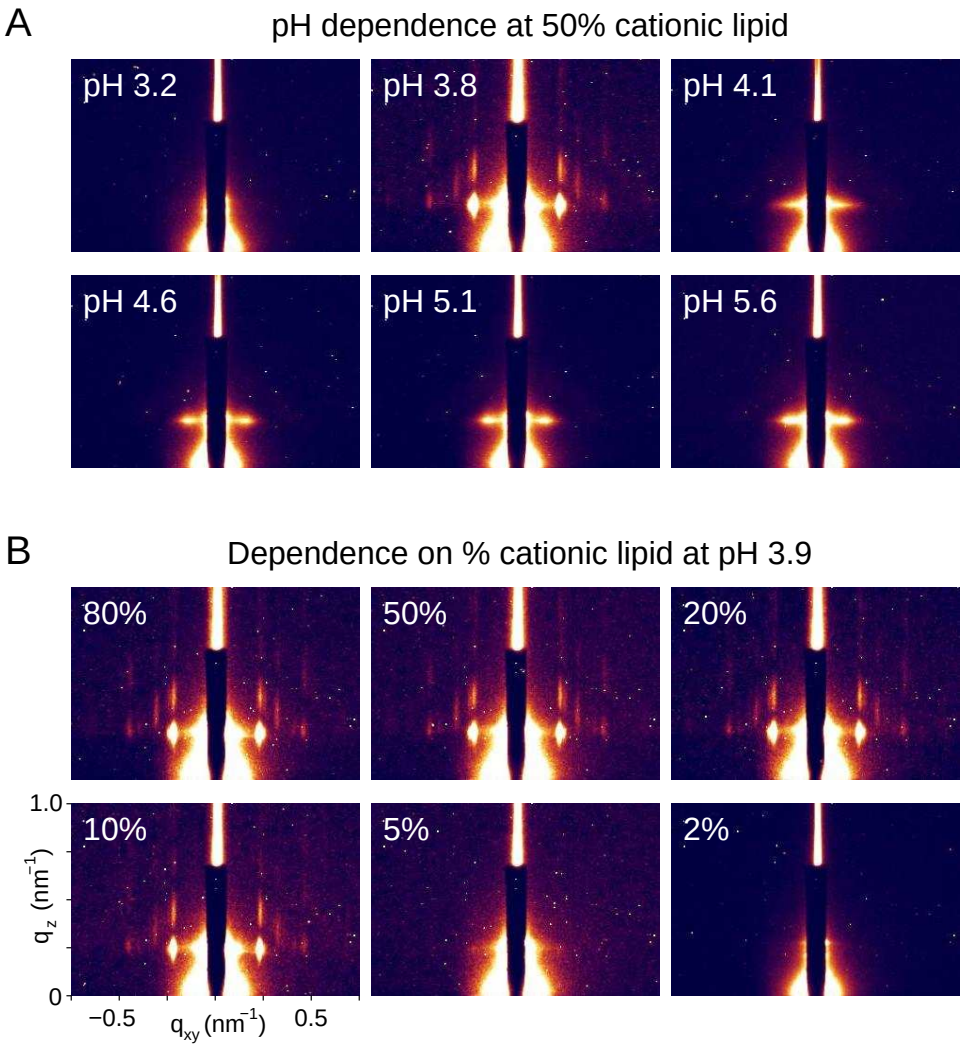

FIG. S2: Low-resolution GISAXS patterns measured (A) at various solution pH at a fixed cationic lipid fraction of 0.5 and (B) at different values of the cationic lipid fraction at pH 3.9 (0.015 mg/ml TYMV).

III. NUMERICAL ANALYSIS FOR CRYSTALLINE 2D PACKING OF MODEL VIRUS-SHAPED PARTICLES

Our x-ray measurements revealed 2D crystals of TYMV and their unit-cell dimensions, but the details of the packing arrangements could not be resolved. To gain further insight to the nature of the observed 2D crystals, we examine the structures of ordered 2D arrays that can be generated numerically using a model virus-shaped particle.

A. Geometric model for TYMV

The icosahedral TYMV particle (Fig. S3(a)) is characterized by knobs of two types: 12 pentagonal knobs (blue) along the 5-fold axes and 20 hexagonal knobs (green and yellow) along the 3-fold axes. These knobs are denoted as "5knobs" and "3knobs," respectively.

Our first task is to construct a simple geometrical model of the virus particle that can be used to study 2D packing of virus-shaped particles. To this end, we represent the virus

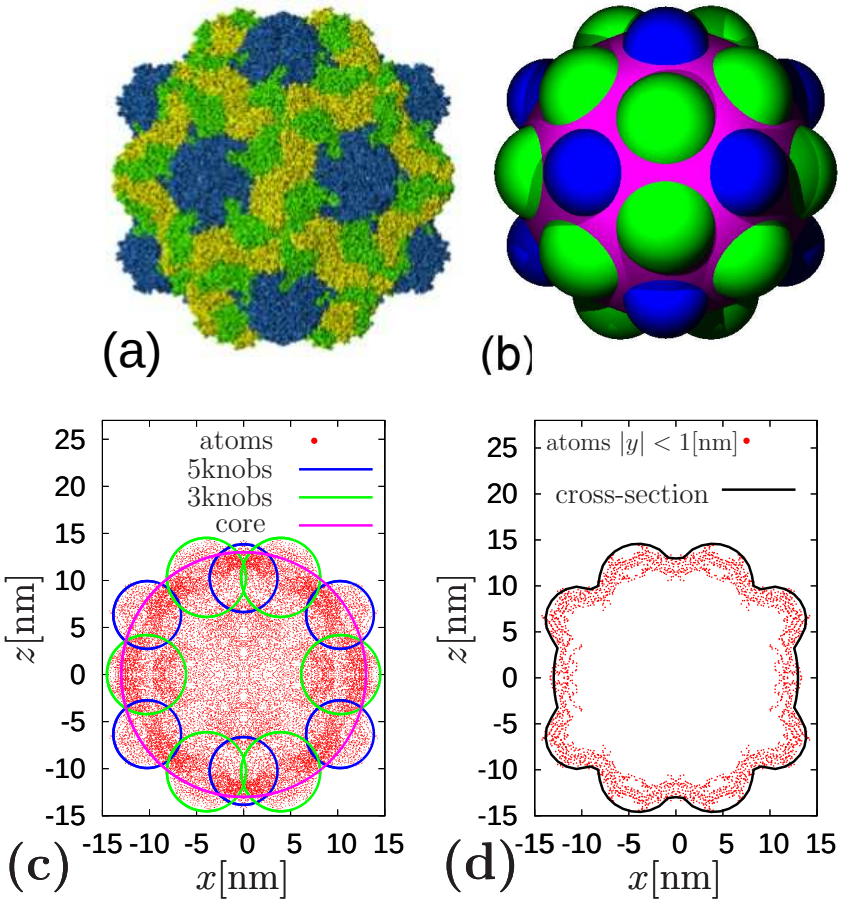

FIG. S3: (a) TYMV particle as viewed along a 2-fold axis. (b) The 3D model of the virus particle. The magenta, blue, and green spheres represent the core, pentagonal knobs ("5knobs"), and hexagonal knobs ("3knobs"), respectively. (c) Projections along the 2-fold axis of the virus atoms [3, 4] (red dots), the core sphere (magenta), selected 5knob spheres (blue), and selected 3knob spheres (green). (d) Projections along the 2-fold axis of the virus atoms near the equatorial (x-z) plane ($|y| < 1$ nm) and the equatorial cross-section of the model particle surface (line).

particle *three-dimensionally* by a combination of spherical components (Fig. S3(b)-(d)). The 5knobs (3knobs) are represented by spheres of radius a_5 (a_3) whose centers lie on the icosahedral 5-fold (3-fold) axes at a distance R_5 (R_3) from the particle center, respectively. The core of the particle is represented by a sphere of radius R. Comparison with the known atomic coordinates of TYMV [3, 4] shows that the size and shape of the virus are well captured by the following parameter choices: $a_5 = 3.6$ nm, $a_3 = 4.2$ nm, $R_5 = 12.04$ nm, $R_3 = 11.05$ nm, and $R = 13.0$ nm. This is demonstrated in Fig. S3(c) and (d), which compare projections of the virus atoms with the model particle.

B. Interaction potentials

To explore packing of the model particles through simulations, we define interparticle interactions. For simplicity, we neglect the chemical and electrostatic heterogeneities of the TYMV particle and employ a "homogeneous" interparticle potential whose anisotropic nature arises solely from the particle shape. Specifically, we represent the 3D interaction between two neighboring model particles by the sum of pair interactions between their spherical components. The latter interactions are set such that they depend only on the component radii and the inter-component distances; they are otherwise independent of the component types (5knob, 3knob, or core). The interaction range chosen is short enough that only the exterior surfaces of the model particle participate in the interactions.

Let R_i denote the radius of a component from one particle, R_j the radius of a component from another neighboring particle, and $r_{ij} = |\vec{r}_i - \vec{r}_j|$ the center-to-center distance between these two components. We consider two types of interactions:

- The hard-core repulsion with the inter-component potential

$$U_{\rm hc}(r_{ij}) = \theta(R_i + R_j - r_{ij}) \tag{1}$$

where $\theta(x) = \begin{cases} 0, x < 0 \\ 1, x > 0 \end{cases}$ is the Heaviside theta function. The interparticle potential based on Eq. (1) is zero if the envelope surfaces of the two interacting particles do not intersect and is non-zero for two intersecting particles. We use this potential to determine the maximum possible packing densities for the model particles.

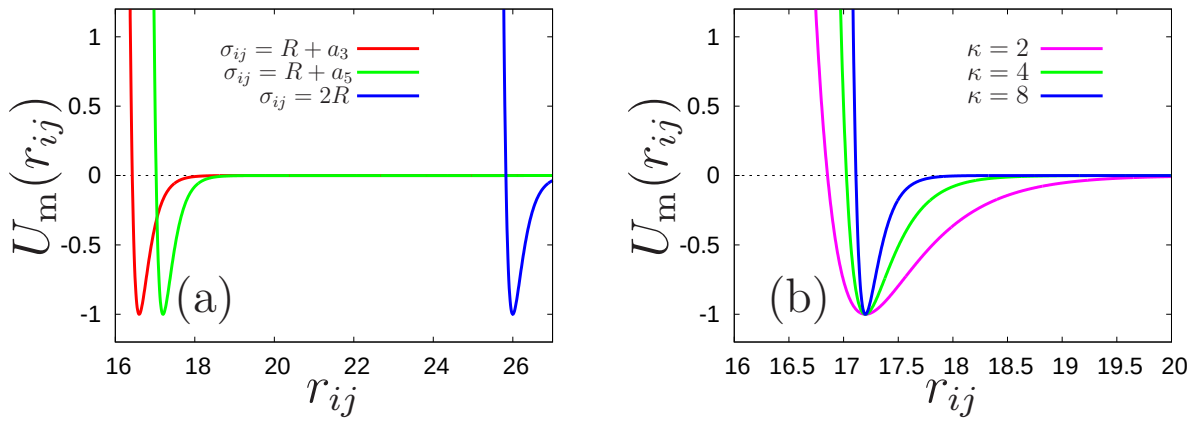

FIG. S4: Examples of the Morse potential: (a) for fixed $\kappa = 4$ nm^{-1} and $\sigma_{ij} = R + a_5, R + a_3, 2R$ for the core-5knob, core-3knob, and core-core interactions, respectively; (b) for $\kappa = 2, 4, 6$ nm^{-1} and fixed $\sigma_{ij} = R + a_3 = 17.2$ nm.

- The Morse potential for the inter-component interactions:

$$U_{\rm m}(r_{ij}) = U_0 \exp(\kappa(\sigma_{ij} - r_{ij}))[\exp(\kappa(\sigma_{ij} - r_{ij})) - 2], \tag{2}$$

  where κ sets the steepness of the potential and $\sigma_{ij} = R_i + R_j$ is the inter-component distance at the potential minimum, corresponding to the two spherical components making a stable contact. The potential is repulsive for $r_{ij} < \sigma_{ij}$ and attractive for $r_{ij} > \sigma_{ij}$. We use this potential to generate contact-optimizing packing arrangements for the model particle through energy minimization.

Fig. S4(a) plots examples of the Morse potential for $\kappa = 4$ nm^{-1} and $\sigma_{ij} = R + a_5, R + a_3, 2R$ for the core-5knob, core-3knob, and core-core interactions, respectively. Since the interactions are treated as homogeneous (*i.e.*, the same U_0 and κ in Eq. (2) for all component pairs), the potential profile is independent of the component types involved. Fig. S4(b) plots the Morse potential for $\sigma_{ij} = R + a_3 = 17.2$ nm and $\kappa = 2, 4, 8$ nm^{-1}. In general, smaller values of κ lead to higher efficiency for the numerical minimization of the interaction energy. Since the effective range for hydrophobic interactions should be about the size of the water molecule ($\sim$0.3 nm), we set $\kappa = 4$ nm^{-1} in the simulations to be described below.

C. Constraints and parameterization for 2D crystal lattices

Our aim is to investigate ordered 2D packing of the model particles with well-defined particle orientations. To facilitate the analysis, we impose the following constraints. First, we assume that the particle centers are confined to the x-y plane such that no particles display out-of-plane displacements along the z axis. The 3D nature of the interparticle interactions is still preserved. Second, we assume that the vertical (normal-to-lattice) orientation of the particle is fixed and consider only the following four cases:

(i) The particle's 2-fold axis is aligned with the z axis.

(ii) The particle's 3-fold axis is aligned with the z axis.

(iii) The particle's 5-fold axis is aligned with the z axis.

(iv) The bisector between adjacent 3-fold and 5-fold axes is aligned with the z axis.

Physical plausibility of these possible orientations is discussed in the main text. With these constraints, the model particle has 3 degrees of freedom: translation in the x-y plane and rotation about the z axis. Since the particle is anisotropic, the interparticle interaction depends on mutual particle orientation.

Third, we only consider 2D crystals with one-particle or two-particle unit cells:

- A crystal with an one-particle (1p) unit cell (see Fig. S5(a)) is characterized by the two lattice constants a_1 and a_2, the lattice angle γ, and the in-plane orientation angle of the particle ϕ. The area per particle is $S = a_1 a_2 \sin(\gamma)$. Thus, for a given S, we can characterize the structure of a 1p crystal by a set of three parameters $\{a_1, \gamma, \phi\}$.

- A crystal with a two-particle (2p) unit cell (see Fig. S5(b)) contains both the first particle (red) with the in-plane orientation angle ϕ_1 and the second particle (blue) with the orientation angle ϕ_2. For the 2p cell, the area per particle is given by $S = \frac{1}{2} a_1 a_2 \sin(\gamma)$. Thus, for a given S, the structure of a 2p crystal is characterized by a set of six parameters $\{a_1, \gamma, \phi_1, \phi_2, x_2, y_2\}$, where (x_2, y_2) are the coordinates for the center of the second particle.

For a given crystal structure, we compute the interaction energy per particle U by performing the sum over all pairs of possible interactions that correspond to the infinite periodic

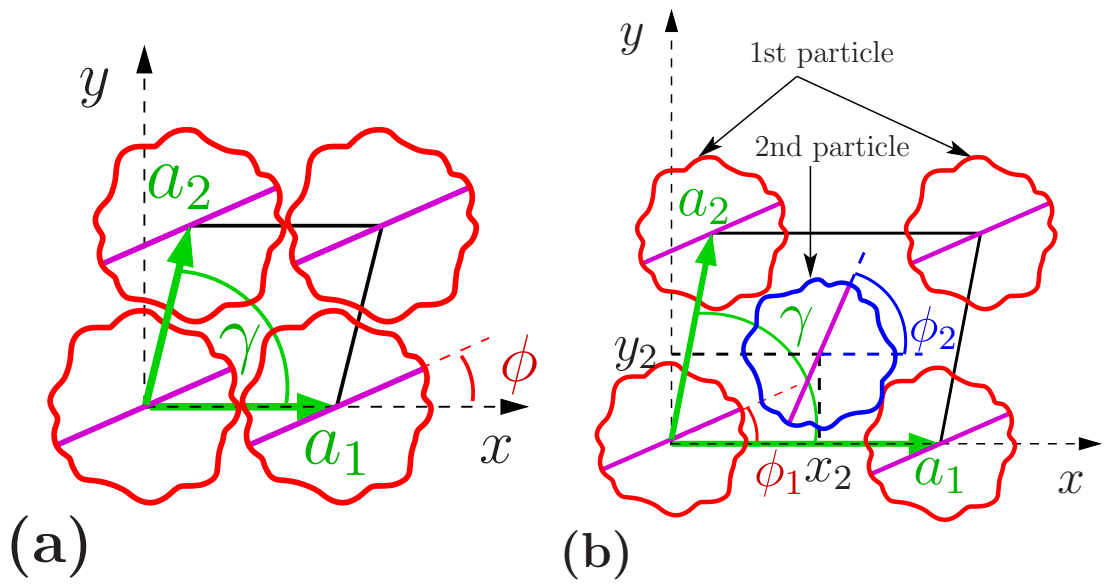

FIG. S5: (a) One-particle (1p) crystal cell with lattice constants a_1 and a_2, lattice angle γ, and particle orientation ϕ. (b) Two-particle (2p) crystal cell with lattice constants a_1 and a_2, lattice angle γ, particle orientations ϕ_1 and ϕ_2, and location of the second particle (x_2, y_2).

structure. The analysis based on the hard-core repulsion (*i.e.,* hard-core interactions of all spherical components of the model particles) is used to generate densest-packing configurations that can be achieved without intersection of the particle surfaces. The analysis based on the Morse potential yields the states with the minimum interaction energy.

D. Densest-packing 1p crystals via the hard-core potential

We examine possible high-density packing arrangements by considering model particles interacting via the hard-core repulsion (Eq. (1)). This potential returns 1 if the surfaces of the two particles intersect and returns 0 otherwise. Our objective is to determine the parameters (a_1, γ, ϕ) for the 1p crystal cell that provides the minimum possible cell area $S_{\min}$ under the condition $U(S, a_1, \gamma, \phi) = 0$, corresponding to non-intersecting particles. We realize this through the following procedure:

1. For given (a_1, ϕ), we examine the dependence of the energy U on the cell area S and the lattice angle γ.

2. As a first step, we check if it is possible to obtain zero interaction energy for a pair

of particles with the orientation ϕ and at the distance a_1. If not, there is no ground state $U = 0$ for the given (a_1, ϕ) and we return to step 1. If yes, proceed to step 3.

3. For a large enough initial value S_t for the cell area, we search for a value γ_t that provides $U(S_t, a_1, \gamma_t, \phi) = 0$. Such a set (S_t, γ_t) exists for large S_t due to step 2. Once a set (S_t, γ_t) is found, proceed to step 4.

4. We decrease the area $S_t^{\rm new} \to S_t - {\rm d}S$ and search for a new value $\gamma_t^{\rm new}$ that provides $U(S_t^{\rm new}, a_1, \gamma_t^{\rm new}, \phi) = 0$. If such $\gamma_t^{\rm new}$ exists, we set $S_t = S_t^{\rm new}$ and $\gamma_t = \gamma_t^{\rm new}$ and repeat this process (step 4). If $U(S_t^{\rm new}, a_1, \gamma_t^{\rm new}, \phi) > 0$ for any $\gamma_t^{\rm new}$, proceed to step 5.

5. At this point, we have $U(S_t, a_1, \gamma_t, \phi) = 0$ (no intersection of particle surfaces) but $U(S_t^{\rm new}, a_1, \gamma_t^{\rm new}, \phi) > 0$ (some intersection) for the smaller area $S_t^{\rm new} = S_t - {\rm d}S$ for any $\gamma_t^{\rm new}$. Thus, the minimum area $S_{\rm min} = S_t$ is provided by the angle $\gamma^* = \gamma_t$ for the given (a_1, ϕ). This procedure defines $S_{\rm min} = S(a_1, \gamma^*, \phi)$.

In general, there is a possibility that for a given $S_{\rm min}$, multiple distinct values of γ^* (corresponding to different cell geometries) may provide $U = 0$. We have checked for this possibility by starting with different values of γ_t in step 3 and comparing the resulting $S_{\rm min}$.

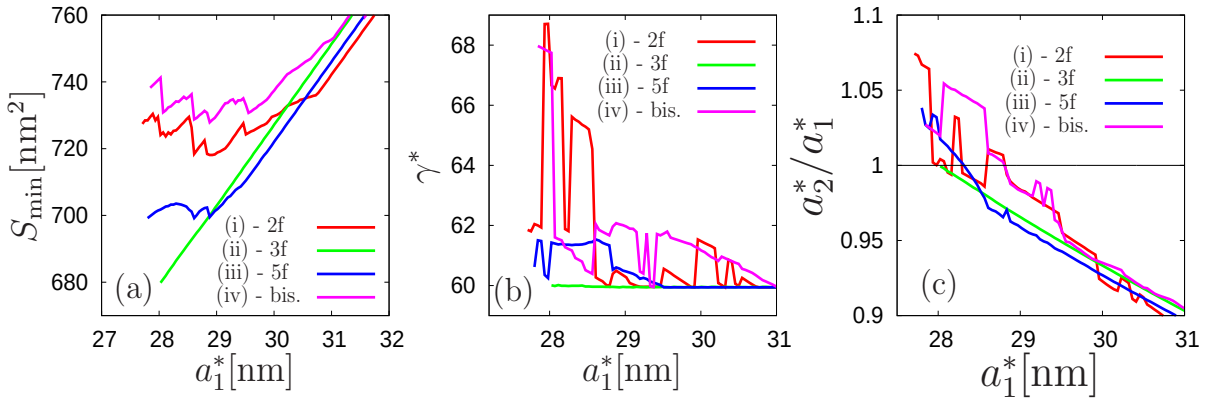

FIG. S6: The 1p crystal parameters for maximum-density configurations as a function of a_1, based on the hard-core potential: (a) the minimum possible area per particle $S_{\rm min}$; (b) the lattice angle γ^* that provides $S_{\rm min}$; (c) the ratio a_2^*/a_1 that provides $S_{\rm min}$. The curves (i), (ii), (iii), and (iv) represent different vertical orientations of the particle, with its 2-fold, 3-fold, 5-fold, and bisector axis aligned along the z axis, respectively.

TABLE I: Parameters of the 1p crystal cell at local minima of the cell area $S_{\rm min}$ (Fig. S6(a)).

orientation	$S_{\rm min}$ [nm^2]	a_1 [nm]	γ^* [°]	ϕ^* [°]	a_2^*/a_1
(i)	718.41	28.61	60.27	30.75	1.0107
(i)	718.11	28.88	60.49	91.35	0.9893
(ii)	679.84	28.025	60.01	9.04	0.9994
(iii)	699.20	27.800	60.62	170.05	1.0383
(iii)	699.20	28.610	61.53	51.55	0.9717
(iii)	699.50	28.880	60.60	70.55	0.9626
(iv)	728.76	28.61	62.05	64.22	1.0079
(iv)	727.86	28.88	62.08	178.19	0.9877

We find that the true $S_{\rm min}$ is given by only one distinct value of γ^*. Thus, the computational procedure used identifies the unique cell geometry for $S_{\rm min}$ at given (a_1, ϕ).

We have extracted the global $S_{\rm min}$ by repeating the above procedure for different sets of (a_1, ϕ). Fig. S6 summarizes the results for different vertical particle orientations (i), (ii), (iii), and (iv), corresponding to the alignment of the icosahedral 2-fold, 3-fold, 5-fold, and bisector axis along the z axis, respectively. Fig. S6(a) shows that several local minima $S_{\rm min}$ exist as a function of a_1. Table I lists the crystal cell parameters for the most prominent of these minima. From Table I, the following observations can be made:

- The densest configurations consist of nearly hexagonal packing ($\gamma^* \sim 60°$, $a_2^*/a_1 \sim 1.0$).
- These configurations exhibit $S_{\rm min} = 680$ to 728 nm^2/particle, depending on the particle orientation; that is, they are substantially denser than the observed 2D crystals ($S_{\rm obs} \approx$ 770 nm^2/particle).
- The maximum possible density is $S_{\rm min} = 680$ nm^2/particle, obtained for the vertical orientation of the particle's 3-fold axis.

E. Ground states for 1p crystals via the Morse potential

The ground state of the system of particles interacting via the Morse potential (Eq. (2)) corresponds to the crystal lattice with the minimum interaction energy per particle. For a

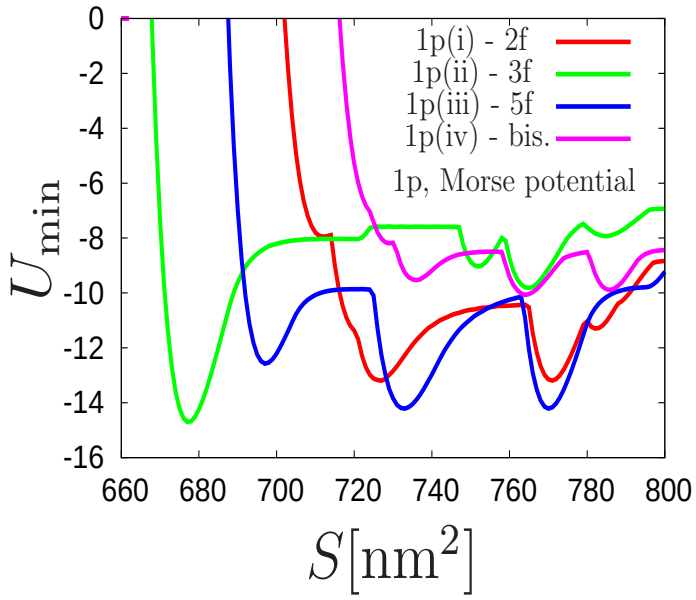

FIG. S7: The minimum energy $U_{\min}$ (via the Morse potential) as a function of the area/particle S for 1p crystals with different vertical particle orientations (i), (ii), (iii), and (iv).

given area per particle S, the geometry of a 1p crystal is defined by the parameters $\{a_1, \gamma, \phi\}$. We have identified a set of parameters $(a_1^*, \gamma^*, \phi^*)$ that provides the minimal energy $U_{\min} = U(a_1^*, \gamma^*, \phi^*) = \min_{\{a_1,\gamma,\phi\}} [U(a_1, \gamma, \phi)]$ by performing direct energy minimization on a grid within ranges $\pi/3 \leq \gamma \leq \pi/2$, $\sqrt{S/\sin(\gamma)} \leq a_1 \leq 1.3\sqrt{S/\sin(\gamma)}$ (*i.e.*, $a_2 \leq a_1 \leq 1.7a_2$, where $a_2 = S/[a_1 \sin(\gamma)]$), and $0 \leq \phi \leq \pi$. Fig. S7 plots the minimal energy $U_{\min}$ as a function of S for different vertical particle orientations (i)-(iv). It can be seen that each $U_{\min}(S)$ curve displays well-defined local minima. The 1p crystal parameters $\{S, a_1^*, \gamma^*, \phi_1^*\}$ for the local minima are listed in Table II, together with the cell aspect ratio a_2^*/a_1^*.

This analysis reveals:

- Most of the local-minimum 1p configurations are close to being rhombic ($a_2^*/a_1^* \sim 1$). But most of these show large deviations in S and/or γ^* as compared to the experimentally observed rhombic crystal ($S_{\mathrm{Rh}} = 772$ nm^2/particle, $a_1 = a_2 = 28.0$ nm, and $\gamma = 80°$).

- The local-minimum 1p configuration for orientation (ii) with $S = 765$ nm^2/particle ($a_1^* = a_2^* = 28.0$ nm, $\gamma^* = 78.0°$) is the most consistent with the observed rhombic crystal. In this configuration, the particle's 3-fold axis is oriented vertically; the anal-

TABLE II: Parameters of the 1p crystal cell at local minima of the interaction energy $U_{\min}$ (Fig. S7).

orientation	S [nm^2]	$U_{\min}$	a_1^* [nm]	γ^* [°]	ϕ^* [°]	a_2^*/a_1^*
(i)	727	-13.1960	27.9415	70.46	170.00	0.9881
(i)	771	-13.1940	27.9386	88.50	9.01	0.9881
(i)	782	-11.2969	28.1893	83.51	74.41	0.9905
(ii)	677	-14.7016	27.9510	60.06	69.01	1.0000
(ii)	752	-9.0346	29.4675	60.00	158.74	1.0000
(ii)	765	-9.8197	27.9671	77.98	69.01	1.0000
(ii)	785	-7.9294	29.4629	72.32	141.26	0.9491
(iii)	697	-12.5759	28.5600	61.563	87.57	0.9717
(iii)	733	-14.2127	27.7510	72.02	81.98	1.0000
(iii)	770	-14.2129	27.7567	88.07	98.0	1.0000
(iv)	736	-9.5303	28.614	68.17	36.76	0.9683
(iv)	764	-10.0691	28.3692	76.47	45.04	0.9763
(iv)	786	-9.8885	28.4814	84.81	116.2	0.9729

ysis further shows that the in-plane particle orientation ($\phi^* = 69.0°$) is such that one of the particle's equatorial 2-fold axes points toward the *next*-nearest neighbors. As described in the main text, this configuration forms the basis for our model of the observed rhombic crystal.

F. Ground states for 2p crystals via the Morse potential

Because of the anisotropic interparticle interactions, the additional degrees of freedom in 2p crystals (Fig. S5(b)) are expected to result in lower interaction energies than for 1p crystals. For this reason, we have performed numerical energy-minimization analysis on 2p cells of particles interacting via the Morse potential (Eq. (2)). In this case, for a given area per particle $S = \frac{1}{2}a_1 a_2 \sin(\gamma)$, we search for minima of the interaction energy $U_{\min}$ in the six-dimensional parameter space $\{a_1^*, \gamma^*, \phi_1^*, \phi_2^*, x_1^*, x_2^*\}$. Note that the two basis particles may have different orientations ϕ_1 and ϕ_2, and that the position of the second particle (x_2, y_2) may deviate from the cell center. We used the following method for this analysis.

For each given S, we randomly selected 40 000 initial points within intervals $\gamma \in [\pi/3, \pi/2]$, $a_1 \in [\sqrt{2S/\sin(\gamma)}, 1.3\sqrt{2S/\sin(\gamma)}]$, $\phi_1 \in [0, \pi]$, $\phi_2 \in [0, \pi]$, $r_x \equiv 2x_2/(a_1 + a_2\cos(\gamma)) \in [0.8, 1.2]$, and $r_y \equiv 2y_2/(a_2\sin(\gamma)) \in [0.8, 1.2]$, where $a_2 = 2S/(a_1\sin(\gamma))$, and the normalized coordinates (r_x, r_y) measure the deviation of the second basis particle from the cell center, at which $(r_x, r_y) = (1, 1)$. Then we performed numerical minimization of the energy using Nelder and Mead simplex algorithm using GNU Scientific Library.

Fig. S8 plots the extracted minimum interaction energy $U_{\min}$ for 2p cells (solid lines) as a function of the area per particle S. For comparison, Fig. S8 also reproduces the results for 1p cells (dashed lines). As expected, for each vertical particle orientation (i)-(iv), the 2p cell yields lower interaction energies than the 1p cell. The parameters for prominent local minima in $U_{\min}(S)$ for the 2p cells are listed in Table III. For a centered 2p cell, *i.e.*, if $(r_x, r_y) = (1, 1)$, the particle positions can be described in terms of an effective 1p cell, as shown in Fig.S9; the corresponding 1p cell parameters are given by: $a_1^{1p} = 1/2\sqrt{(a_1 + a_2\cos(\gamma))^2 + (a_2\sin(\gamma))^2}$, $a_2^{1p} = 1/2\sqrt{(a_1 - a_2\cos(\gamma))^2 + (a_2\sin(\gamma))^2}$, and $\gamma^{1p} = \arcsin(S/(a_1^{1p}a_2^{1p}))$. These parameters

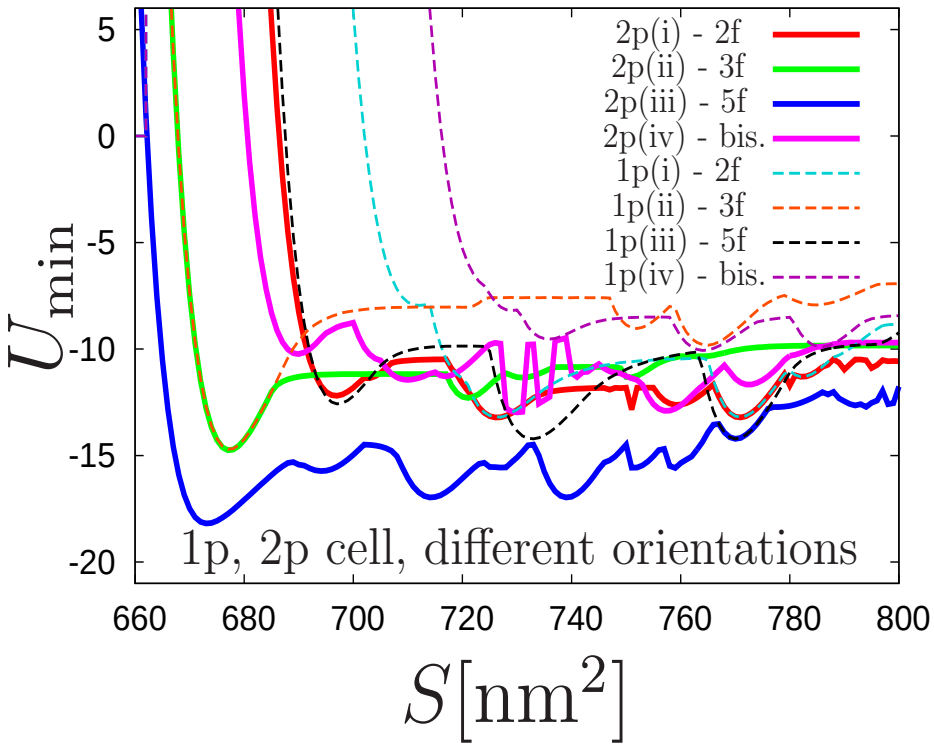

FIG. S8: The minimum energy $U_{\min}$ (via the Morse potential) as a function of the area/particle S for 2p crystals (solid lines) and 1p crystals (dashed lines) with different vertical particle orientations (i), (ii), (iii), and (iv).

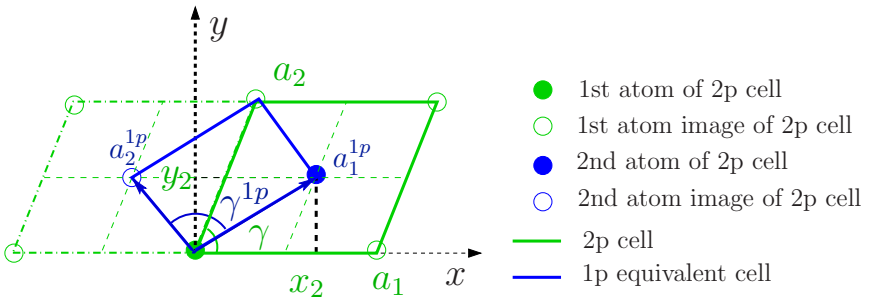

FIG. S9: The geometry of a centered 2p cell (green) and its 1p-equivalent cell (blue).

TABLE III: Parameters of the 2p crystal cell at local minima of the interaction energy $U_{\min}$ (Fig.S8). For centered 2p cells ($(r_x, r_y) = (1, 1)$), the equivalent 1p-cell parameters $\{a_1^p, a_2^p, \gamma^p\}$ are provided.

orientation	S [nm^2]	$U_{\min}$	γ^* [°]	a_1^* [nm]	a_2^*/a_1^*	r_x	r_y	γ^{1p} [°]	a_1^{1p} [nm]	a_2^{1p} [nm]	a_2^{1p}/a_1^{1p}
(i)	697.0	-12.1958	90.00	50.498	0.547	1.000	1.000	57.33	28.775	28.775	1.000
(i)	726.0	-13.2136	89.30	45.388	0.705	1.000	1.000	70.36	27.925	27.604	0.989
(i)	771.0	-13.2140	90.67	39.775	0.975	1.000	1.000	88.53	27.611	27.933	1.012
(ii)	677.0	-14.7468	90.00	48.428	0.577	1.000	1.000	60.00	27.960	27.959	1.000
(ii)	721.0	-12.2937	81.05	52.198	0.536	0.923	0.727	N/A	N/A	N/A	N/A
(ii)	731.0	-11.3422	95.47	52.520	0.532	0.914	1.166	N/A	N/A	N/A	N/A
(iii)	673.0	-18.1881	90.00	46.561	0.621	1.000	1.000	63.67	27.403	27.403	1.000
(iii)	714.0	-16.9638	90.00	44.346	0.726	1.000	1.000	71.97	27.402	27.402	1.000
(iii)	739.0	-16.9662	90.00	42.053	0.836	1.000	1.000	79.78	27.403	27.403	1.000
(iii)	770.0	-14.2158	90.00	39.900	0.967	1.000	1.000	88.10	27.757	27.756	1.000
(iv)	710.0	-11.4476	84.68	50.268	0.564	1.000	1.000	58.77	29.985	27.691	0.923
(iv)	730.0	-12.9751	78.29	53.824	0.515	1.000	1.000	53.89	32.671	27.656	0.847
(iv)	757.0	-12.8992	90.00	41.750	0.869	1.000	1.000	81.95	27.650	27.650	1.000
(iv)	773.0	-11.6667	90.00	40.533	0.941	1.000	1.000	86.52	27.829	27.828	1.000

are also listed in Table III where applicable.

From Fig. S8 and Table III, we conclude:

- Most of the local-minimum 2p configurations consist of centered 2p cells ($(r_x, r_y) = 1$) and are nearly rhombic ($a_2^{1p}/a_1^{1p} = 1$).

- The two highest-density 2p configurations are given by orientation (iii) with $S = 673$ nm^2/particle and orientation (ii) with $S = 677$ nm^2/particle. Both of these are close to being hexagonally packed ($\gamma^{1p} \sim 60°$, $a_2^{1p}/a_1^{1p} = 1$). Their densities and hexagonal nature are consistent with the results based on the hard-core potential ($S_{\min} \approx 680$ nm^2/particle; see Table I).

- Nevertheless, none of the local-minimum 2p configurations resembles the two experimentally observed 2D crystals, namely, the (2×1) rectangular crystal ($S_{\rm rec} = 767$ nm^2/particle, $a_2/a_1 = 0.5$, $\gamma = 90°$) and the rhombic crystal ($S_{\rm Rh} = 772$ nm^2/particle, $a_2^{1p}/a_1^{1p} = 1.0$, $\gamma^{1p} = 80°$).

---

[1] S. Kewalramani, S. T. Wang, Y. Lin, H. G. Nguyen, Q. Wang, M. Fukuto, and L. Yang, Soft Matter **7**, 939 (2011).

[2] G. Kaur, J. He, J. Xu, S. V. Pingali, G. Jutz, A. Boker, Z. Niu, T. Li, D. Rawlinson, T. Emrick, et al., Langmuir **25**, 5168 (2009).

[3] S. B. Larson, R. W. Lucas, A. Greenwood and A. McPherson, *Virology*, 2005 **334**, 245-254. PDB ID: 2FZ2.

[4] H. M. Berman, J. Westbrook, Z. Feng, G. Gilliland, T. N. Bhat, H. Weissig, I. N. Shindyalov and P. E. Bourne, *Nucleic Acids Res.*, 2000, **28**, 235-242. http://www.pdb.org.